Sun glint estimation in marine satellite images: a comparison of results from calculation and radiative transfer modeling

Susan Kay,[1,4,*] John Hedley,[2] and Samantha Lavender[3]

[1]College of Life and Environmental Sciences, University of Exeter, Prince of Wales Road, Exeter EX4 4PS, UK

[2]ARGANS Ltd, Tamar Science Park, 1 Davy Road, Plymouth PL6 8BX, UK

[3]Pixalytics Ltd, Tamar Science Park, 1 Davy Road, Plymouth, Devon, PL6 8BX, UK

[4]Present address: Plymouth Marine Laboratory, Prospect Place, The Hoe, Plymouth PL1 3DH, UK

*Corresponding author: suka@pml.ac.uk

Received 10 May 2013; accepted 19 June 2013;
posted 8 July 2013 (Doc. ID 189886); published 5 August 2013

The intensity and location of Sun glint in two Medium Resolution Imaging Spectrometer (MERIS) images was modeled using a radiative transfer model that includes elevation features as well as the slope of the sea surface. The results are compared to estimates made using glint flagging and correction approaches used within standard atmospheric correction processing code. The model estimate gives a glint pattern with a similar width but lower peak level than any current method, or than that estimated by a radiative transfer model with surfaces that include slope but not height. The MERIS third reprocessing recently adopted a new slope statistics model for Sun glint correction; the results show that this model is an outlier with respect to both the elevation model and other slope statistics models and we recommend that its adoption should be reviewed. © 2013 Optical Society of America

OCIS codes: (010.0010) Atmospheric and oceanic optics; (010.4450) Oceanic optics; (010.5620) Radiative transfer.

http://dx.doi.org/10.1364/AO.52.005631

1. Introduction

Sun glint consists of light that has been directly reflected from the sea surface into a satellite sensor, without ever entering the water. In Sun glint contaminated regions the glint signal is typically much larger than the below-water signal, which makes retrieval of variables such as chlorophyll concentration difficult or impossible. Sun glint is a serious problem for marine satellite imagery, causing large amounts of ocean color data loss, particularly for sensors that do not tilt to avoid the worst glint, such as the Medium Resolution Imaging Spectrometer (MERIS) and Moderate Resolution Imaging Spectroradiometer (MODIS); see Fig. 2 below for an example of glint contamination in two MERIS images. However, Sun glint data can be important for applications such as oil slick detection [1], so making all sensors tilt away from Sun glint is not the solution.

Some correction of Sun glint is implemented in the standard atmospheric correction code for a number of ocean color satellites, including MERIS and MODIS. The current method relies on geometry: for each pixel, the sea surface is divided into many small facets and an estimate is made of the fraction of the facets that are orientated to reflect light directly from the Sun to the satellite. From this the radiance (or reflectance) due to Sun glint can be calculated and subtracted from the radiance measured by the sensor [2,3]; see Subsection 2.B. The calculation requires

1559-128X/13/235631-09$15.00/0

the probability distribution function (PDF) of the sea surface facet slopes, which can be calculated from the wind speed using the well-known model of Cox and Munk [4,5] or later variants [6,7]. Zhang and Wang [8] compared the results obtained using a number of sea surface-slope–wind-speed relationships for a limited number of MODIS images and concluded that the model of Cox and Munk was the most accurate for estimation of Sun glint.

Other glint correction methods are under investigation and showing some promise [9,10]; a neural network method is available for MERIS processing for Case 2 waters [11] and the POLYMER algorithm [9] has currently been chosen as the atmospheric correction code of choice for MERIS processing within the ESA Ocean Color Climate Change Initiative project [12]. However, for the moment the slope statistics method is the standard approach used in the atmospheric correction code for processing Case 1 waters.

Slope statistics methods are also used to model the water surface in radiative transfer models such as Hydrolight [13]. These models can make good estimates of the directional reflection and refraction of light at the water surface, but they assume zero elevation, i.e., that the sea surface is at its equilibrium height everywhere. Therefore they cannot include elevation-dependent processes such as multiple interactions at the water surface and the shadowing effect of tall waves. Use of an air–water interface that includes the elevation as well as the slope of the sea surface can alter the results of radiative transfer models [14] and so could contribute to better estimation of Sun glint.

In this study a radiative transfer model with an elevation-based air–water interface was used to estimate the intensity and location of Sun glint corresponding to two MERIS images. The results were compared to estimates made using radiative transfer modeling with a slope-statistics interface and to calculations using the current standard method as used in atmospheric correction code, with various versions of the wind–surface slope relationship:

- The original model of Cox and Munk [4], as used for MERIS data processing until Summer 2011 [15];
- The model of Ebuchi and Kizu [6], which has been adopted for MERIS data processing at the third reprocessing (2011) [3];
- The method of the third MERIS reprocessing, but using the model of Bréon and Henriot [7];
- A simplified version of the Cox and Munk model, without wind speed dependence: this is used in data processing for SeaWiFS and MODIS [2];
- Another variation on Cox and Munk, as used for Hydrolight [16].

Section 2 describes the methods used and the two images chosen for this case study. Section 3 compares the results from the various methods and Section 4 presents a summary and conclusions.

2. Methods

Seven estimates of the Sun glint pattern in sections from two MERIS images were made, using two types of method: radiative transfer modeling and the approach used within standard atmospheric correction code. This section describes these methods, starting with the radiative transfer model, and then the selection and processing of the two images. The seven methods are summarized in Table 1.

A. Methods Used for Radiative Transfer Modeling

The radiative transfer model PlanarRad [17,18] was used to simulate the transfer of light at the water surface by a Monte Carlo technique. Light rays were sent toward the surface from all directions, and the direction and intensity of received light was used to build up a bidirectional reflectance distribution function. Two models of the surface were used:

1. Elevation-based surfaces (Elmodel), which are numerical realizations of the surface with statistics of both slope and elevation matching those of observed seas at a given wind speed. This method has been previously described in [14].
2. A slope-statistics representation (CMmodel), in which each photon encounters a different surface slope, with the distribution of slopes given by the Cox–Munk model. This method has been used in Hydrolight [13] and a number of other radiative transfer models [14], and is described fully in [16].

The elevation-based surfaces were created by Fourier inversion of a unified slope spectrum designed to cover wavelengths from a few millimeters to several hundred meters [19], with a directional spectrum that allowed fully two-dimensional surface realizations to be created [20]. Each surface

Table 1. Summary of Methods for Sun Glint Estimation Described in Subsections 2.A and 2.B

Method	Description	Reference
Elmodel	Monte Carlo modeling at surfaces with both elevation and slope features	[14]
CMmodel	Monte Carlo modeling at slope-statistics surfaces, with the version of the Cox and Munk model used in Hydrolight	[16]
MERIS2	Calculation using the full Gram–Charlier expansion of the slope PDF	[15]
MERIS3	As MERIS2 but using the Ebuchi and Kizu model for the mean square slope	[3,6]
BHcalc	As for MERIS2, but using the PDF of Bréon and Henriot	[7]
SWcalc	As for the SeaWiFS and MODIS algorithm: calculation using a Gaussian PDF and the mean square slope independent of wind direction	[2]
CMcalc	Calculation using a Gaussian PDF with the same Cox–Munk model as the CM surfaces	

realization represented an area of sea 200 m square, with a grid size of 3 mm. At this level of resolution the variance of both sea surface slope and elevation is within the range of those observed in real seas [14]: for example the mean square slope lies within the limits of accuracy of the Cox–Munk model [4]. A coarser grid would omit shorter waves, which contribute substantially to the slope.

The horizontal size of the sea surface realization was on a similar scale to the pixel size for MERIS reduced resolution images (1000 m), so results from an entire surface realization were used to simulate each pixel. The results reported are for the average of ray tracing on ten surface realizations, each time with 5×10^7 rays. The sphere was partitioned into sections ("quads") 10° vertically by 15° horizontally, with two end caps of angular width 5° at the poles, and the horizon quads were further divided into two 5° sections (Fig. 1); this is the same as the partitioning used in standard Hydrolight configurations [13]. Surface files for use in the simulation were created for wind speeds between 3 and 8 $\mathrm{m\,s^{-1}}$, at intervals of 0.5 $\mathrm{m\,s^{-1}}$, with ten surfaces at each speed.

The glint reflectance ρ_g was calculated by using

$$\rho_g = \pi L_g / E_d, \tag{1}$$

where L_g is the upwelling reflected radiance in the direction of the sensor and E_d is the downwelling planar irradiance, both just above the surface; this expression makes the reflectance directly comparable to that obtained from the calculation method [Eq. (2)]. E_d was estimated by using libRadtran [21]. Data for the solar flux and the atmosphere model were taken from the libRadtran library, with the default aerosol options and maritime aerosol in the boundary layer [22]. Values of the ozone column density were taken from the MERIS image data (Subsection 2.C). The irradiance was distributed across the upper hemisphere according to the clear sky model of [23]. L_g is a model output for a given E_d and surface. Note that, since ρ_g depends on the ratio L_g/E_d, the glint reflectance depends only weakly on the atmospheric model chosen.

For the CMmodel simulations the same modeling framework was used, with slope-statistics surfaces replacing the elevation-based surfaces [16].

Two further checks were made on the model. The model glint reflectances were created for a clear sky scenario and include light scattered to the water surface from the atmosphere (sky glint); the MERIS values, calculated by adding contributions to the reflected sunlight from different parts of the surface, do not. The effect of sky glint was assessed by running the model with the same direct irradiance, all in the section of the sphere containing the Sun, and zero irradiance elsewhere. The second check was on the effect of angular resolution. In PlanarRad the minimum angular size is one sphere section; for the results presented above this is $15° \times 10°$ so the modeled Sun is much larger than the real solar disc (diameter 0.5°). To investigate the sensitivity of the model to angular resolution, the model was run with each quad half the size in both directions ($7.5° \times 5°$, and the end caps were reduced to 2.5°). For this run the wind speed was approximated as 5 $\mathrm{m\,s^{-1}}$ for all pixels to reduce processing requirements.

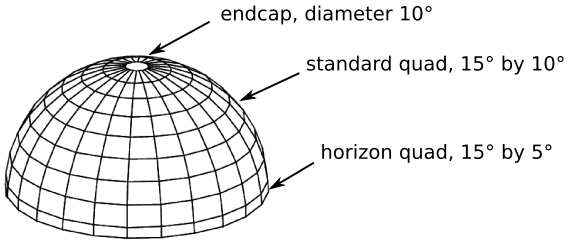

Fig. 1. Diagram to illustrate the division of the sphere used in ray tracing. The lower half of the sphere is divided in the same way.

B. Methods for Calculating Sun Glint

Calculation of Sun glint was as used in standard atmospheric correction code for ocean color sensors, such as SeaWiFS, MODIS, and MERIS [2,3,24]. A PDF was used to estimate the fraction of the sea surface orientated so as to reflect incoming sunlight directly toward the sensor. From this the received glint reflectance was calculated:

$$\rho_{\mathrm{glint}} = \frac{\pi L_{\mathrm{glint}}}{E \cos\theta_s} = \frac{\rho(\omega,\lambda) p(\xi,\eta)}{4 \cos^4\beta \cos\theta_v \cos\theta_s}, \tag{2}$$

where L_{glint} is the reflected radiance just above the surface, E is the downwelling irradiance just above the surface, θ_s and θ_v are the Sun and sensor zenith angles, and β is the slope of a surface facet that will reflect light directly from the Sun to the sensor: it can be calculated from the Sun and viewing geometry. $p(\xi,\eta)$ is the PDF of sea surface slopes; ξ and η are normalized slopes and depend on the Sun and viewing geometry and the wind speed and direction. $\rho(\omega,\lambda)$ is the Fresnel reflection coefficient; ω is the angle of incidence and can be calculated from θ_s and θ_v.

Cox and Munk [4,5] expressed the PDF as a Gram–Charlier expansion with seven parameters. Of these, the mean square slope in the upwind and crosswind directions have received the most attention. Cox and Munk suggested the following relationship between mean square slope and wind speed:

$$\sigma_w^2 = 0.00316U \pm 0.004, \tag{3}$$

$$\sigma_c^2 = 0.003 + 0.00192U \pm 0.002, \tag{4}$$

where σ_w and σ_c are the root mean square slopes in the downwind and crosswind directions and U is the wind speed at 41 feet (12.5 m) above sea level. This model was used for MERIS data processing until Summer 2011, and for the MERIS2 method in the present work. Ebuchi and Kizu [6] used satellite

measurements of subtropical seas to suggest an alternative model, which has been adopted for the calculation of Sun glint in the third MERIS reprocessing [3] (MERIS3):

$$\sigma_w^2 = 0.0053 + 0.000671U_{10}, \quad (5)$$

$$\sigma_c^2 = 0.0048 + 0.00152U_{10}. \quad (6)$$

Bréon and Henriot [7] also used satellite measurements, but with global coverage. Their mean square slope model is

$$\sigma_w^2 = 0.001 + 0.00316U_{10} \pm 0.00005, \quad (7)$$

$$\sigma_c^2 = 0.003 + 0.00185U_{10} \pm 0.00005. \quad (8)$$

They also give slightly altered values for the other Gram–Charlier parameters. These values were used in the BHcalc method.

Glint correction in SeaWiFS and MODIS processing (SWcalc) uses only the Gaussian terms of the PDF and omits dependence on the wind direction:

$$\sigma_w^2 = \sigma_c^2 = 0.00246U_{10}. \quad (9)$$

Hydrolight also uses a Gaussian PDF, with a version of the mean square slope formula without any offsets:

$$\sigma_w^2 = 0.00316U_{10}, \qquad \sigma_c^2 = 0.00192U_{10}. \quad (10)$$

This PDF was used for the CMcalc results.

C. Simulation of Glint in MERIS Images

The methods described above were applied to simulate Sun glint for across-swath lines from two MERIS images (Fig. 2). The images were chosen to have only small amounts of cloud, and winds speeds of 5–8 m s^{-1}; so foam on the sea surface was negligible [25]. In both cases the line extends from an area of low glint (left-hand side of the image) into the peak glint area. The Mediterranean image is for a higher latitude and has a closer proximity to land. The aerosol optical thickness as retrieved by the MERIS algorithm was around 0.05–0.1 for most pixels in the Atlantic image and 0.1–0.2 for the Mediterranean image.

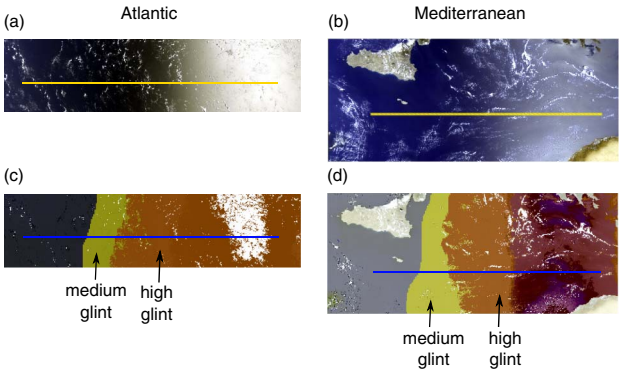

Fig. 2. Parts of two MERIS images, showing the lines chosen for simulation. (a) and (c) Atlantic Ocean, 35° 26′ 20″ W, 25° 6′ 52″ S to 27° 26′ 28″ W, 26° 46′ 5″ S, 31 December 2003. (b) and (d) Mediterranean Sea, 13° 0′ 20″ E, 35° 41′ 33″ N to 22° 9′ 54″ E, 33° 49′ 57″ N, 31 July 2006. (a) and (b) show level 1 RGB images, (c) and (d) show level 2 images with the medium and high glint pixels flagged in the center and on the right of the image.

The glint reflectance was estimated for every tenth pixel along the two lines, using the methods in Table 1. Ten MERIS wavelengths were used: 412.69, 442.56, 489.88, 509.82, 559.69, 619.60, 664.57, 680.82, 708.33, and 753.37 nm. Geometry and wind values were taken from the MERIS level 1 data, in which the solar and viewing angles are calculated from orbit information and acquisition time; wind speed and direction are taken from the ECMWF model and interpolated to the MERIS grid [26]. The Fresnel reflection coefficient was taken as 0.022, as used for MERIS data processing [3].

As a check that the model estimates were in line with MERIS measured values, an estimate of the at-sensor radiance was also made for the same set of pixels. For this an in-water section was added to the model, using PlanarRad [17,18], with values of the inherent optical properties selected to suit ocean waters.

3. Results and Discussion

The radiance estimated by the elevation-based model gave a reasonable match to the size and position of the glint signal in the MERIS level 1 values (Fig. 3). The values of the modeled radiance depend strongly on the atmospheric and in-water models, which are out of the scope of this study and will not be discussed further. So a one-to-one matching of the radiance is not considered, but this comparison serves as a basic validation of the model.

The glint signal in the modeled reflectance was in approximate agreement with that calculated using the MERIS glint algorithm, with agreement better for the second reprocessing values than the third (Fig. 4; see also Fig. 6). The reflectances had only a weak dependence on wavelength: reflection at the water surface is wavelength dependent only through the refractive index, which was taken as constant for this model, consistent with the MERIS treatment of the Fresnel reflectance as a wavelength-independent constant [3].

The zenith and azimuth angles of the ingoing and outgoing model quads are shown in the plots below the main sections of Fig. 4; these refer to the quad centers. It can be seen that many of the sudden changes in model results occur where there is a move from one quad to another. Other spatial discontinuities in reflectance occur where there is a change from one wind speed level to the next as the wind varies across the image. The vertical lines on the plots show the boundaries of the medium and high

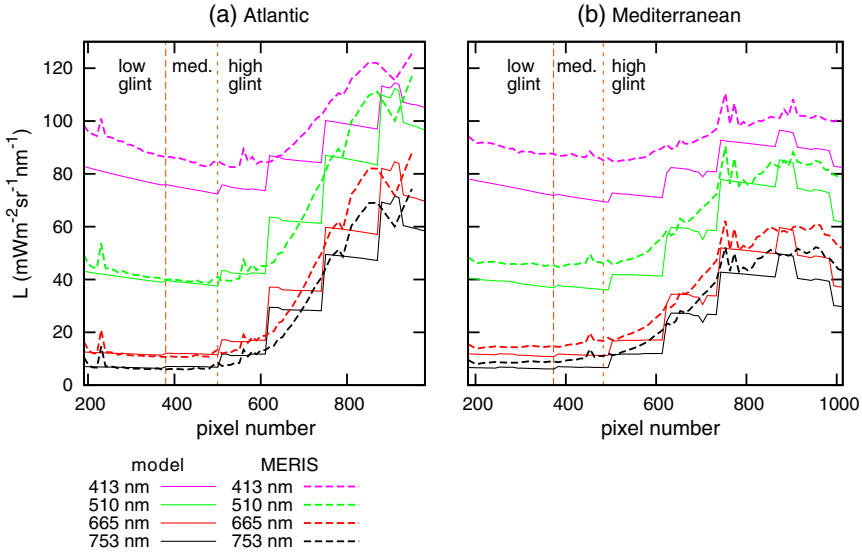

Fig. 3. Level 1 radiance calculated by the model (solid curves) and reported for MERIS (dashed curves) for the two image lines shown in Fig. 2. The model values are the mean for 10 surfaces. Pixels flagged as cloud in the MERIS data have been omitted. The vertical lines show the edges of the MERIS medium and high glint regions, as in Figs. 2(c) and 2(d).

glint regions, as used by the MERIS correction algorithm. Medium glint is a relatively narrow band of the whole glint pattern, illustrating how current approaches address and correct only a relatively small proportion of the image.

Model results using surfaces created by the slope-statistics method gave higher peak glint reflectance, but lower reflectance near the edge of the glint region (Fig. 5, CM model). This is in line with results presented previously [14], which showed that the elevation-based surfaces give reduced forward scattering and enhanced sideways scattering when compared to slope-statistics models. For pixels near the glint peak the Sun and satellite are more directly in line; so the signal is dominated by forward scattering, while sideways scattering influences the edge of the glint pattern.

Comparison of the various calculation methods listed in Table 1 shows broad agreement on the location of the glint pattern (Fig. 6), but with the Ebuchi

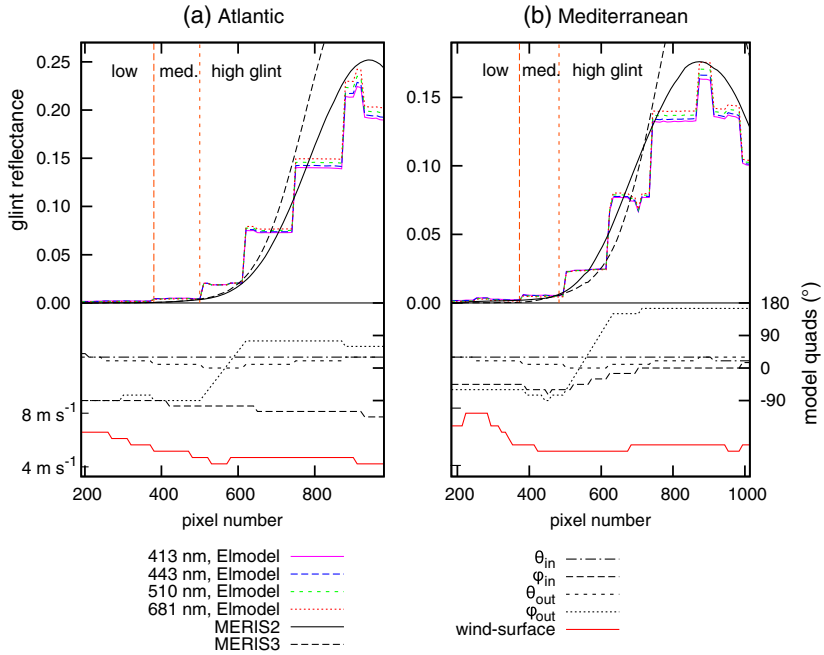

Fig. 4. Glint reflectance at four wavelengths estimated by the elevation-based model and Sun glint reflectance (wavelength independent) calculated as in the MERIS Sun glint algorithm, for the two image lines shown in Fig. 2. The model values are the mean for 10 surfaces. The ingoing and outgoing quads for each pixel and the wind speed used to generate the surface realization are shown below the main plots. The vertical lines show the edges of the MERIS medium and high glint regions.

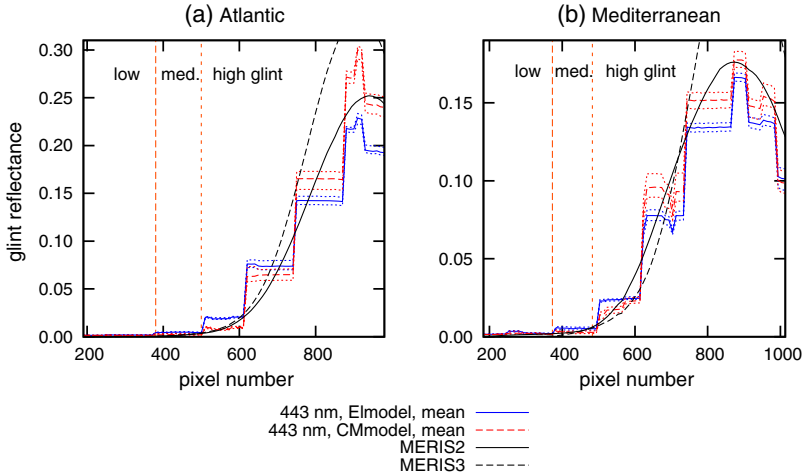

Fig. 5. Glint reflectance at 443 nm estimated by the model using the elevation-based sea surfaces (Elmodel) and slope-statistics surfaces (CMmodel). In each case the central line shows the mean for 10 surfaces; the minimum and maximum are also shown. The smooth curves show the Sun glint reflectance calculated using the MERIS algorithm and the vertical lines show the edges of the medium and high glint regions.

and Kizu model (MERIS3) giving a noticeably taller and narrower pattern than the others. The difference from the other models is less obvious in the medium glint region, which is where the MERIS glint correction is important, and for these two image lines it is not clear whether MERIS3 is better than MERIS2 for medium glint [Figs. 6(c) and 6(d)]. For the Atlantic image the shapes are nearly identical, while in the Mediterranean image the MERIS3 algorithm gives a steeper rise, but the coarse resolution of the simulation makes it difficult to judge which is a better match. The model with the best agreement to that

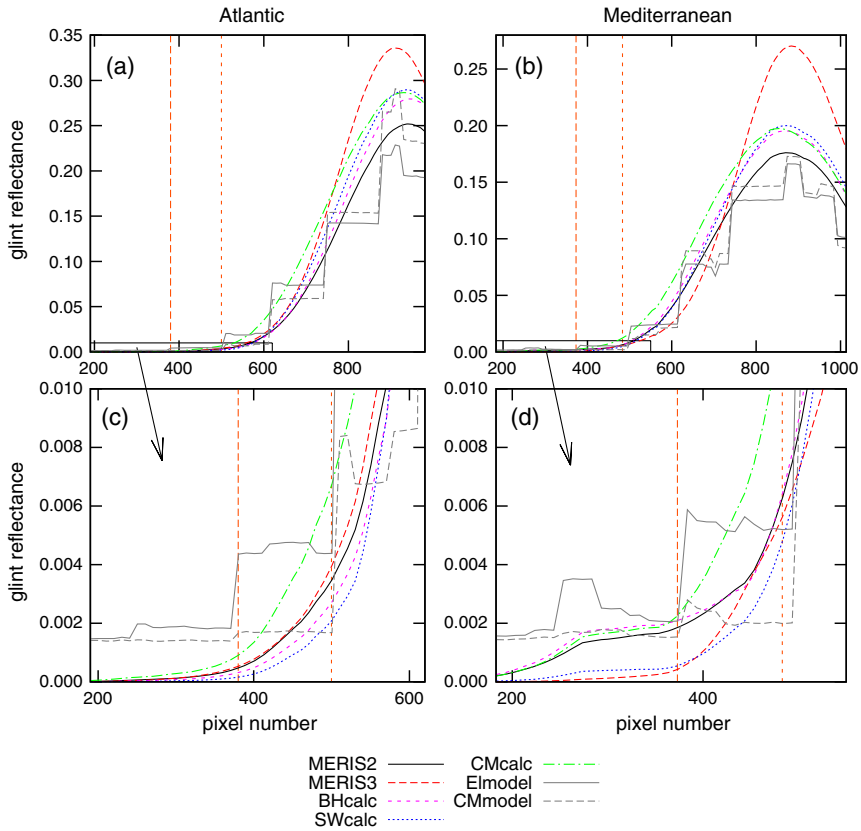

Fig. 6. Glint reflectance (wavelength independent) for the two lines in Fig. 2, calculated by the MERIS method using various parameter values. See the text for details of the different methods. The value estimated by the current model using elevation-based surfaces and CM slope-statistics surfaces is also shown. (a), (c) Atlantic image; (b), (d) Mediterranean image. (a), (b) The full image line; (c), (d) the low and medium glint regions enlarged. The vertical lines show the edges of the MERIS medium and high glint regions.

from radiative transfer modeling at elevation-based surfaces is Cox and Munk (MERIS2), but all the methods give higher peak glint reflectance than Elmodel, and all except CMcalc give a lower value in the medium glint region [Figs. 6(c) and 6(d)]. The medium glint region is important, as this is where correction is currently possible; however the progress made using other approaches, e.g., [9], suggests that correction of higher glint may be possible, and so the aim should be a model with good performance in all parts of the glint pattern. The elevation-based model's agreement with the Cox and Munk model is consistent with the results of Zhang and Wang [8], who also found that Ebuchi and Kizu's values gave the lowest correlation to measurement in their study of MODIS images. The Bréon and Henriot values gave results very similar to the original Cox–Munk values: Bréon and Henriot's values are based on a data set with greater global coverage than that of Ebuchi and Kizu, and so may be more robust. Given that the Ebuchi and Kizu model has appeared as an outlier in both this study and in [8], which used a different method and wavelength range, we suggest that its use for MERIS data processing may need to be reviewed, especially if correction at higher glint levels is desired.

The calculation with the CM/Hydrolight parameters, CMcalc, gave a higher glint reflectance than that estimated by the model using slope-statistics surfaces, CMsurf. This demonstrates that the calculation and ray-tracing methods can give different estimates for the glint reflectance, even when using the same assumptions about the surface and the same PDF.

For all the quantities tested, variation between results from different surface realizations was low compared to variation between the model and MERIS values, or between wavelengths. The data in Fig. 5, which shows values varying within a few per cent of the mean, were typical. This indicates that differences in reflectance due to variation in the sea surface shape are much smaller than those due to other modeled processes, indicating that pixel-to-pixel variation due to the exact position of surface waves within pixels is a minor contributor to noise in MERIS reflectances (see also [14]).

Removal of the sky glint component in the radiative transfer model, by considering direct irradiance only, reduced the reflectance by about 50% in the medium glint zone and about 20% in the highest glint region. The change improves agreement between the model and MERIS2 estimates for the medium glint regions: this is clearest in Figs. 7(c) and 7(d) which show the lower glint regions in greater detail. However, agreement is reduced in the high glint region.

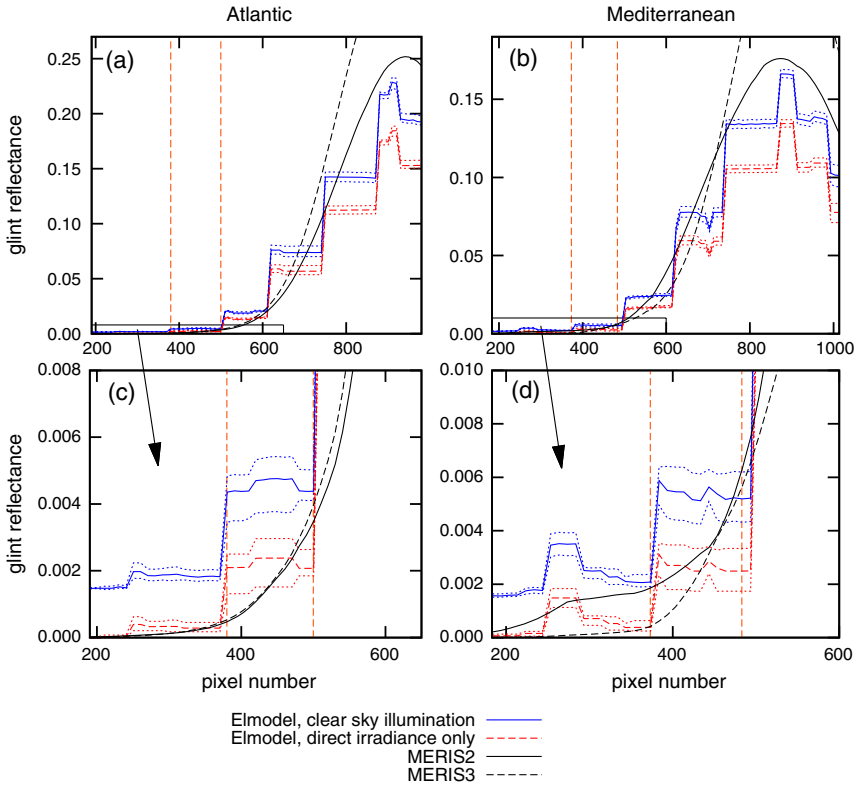

Fig. 7. Modeled glint reflectance at 443 nm for the elevation-based model with standard, clear sky, illumination and for direct irradiance only, with all illumination coming from the quad containing the Sun. (a) Values for the Atlantic image, (b) values for the Mediterranean image, (c), (d) the lower glint regions of (a) and (b) enlarged. Results are the mean for 10 surfaces; the minimum and maximum values are also shown. The smooth curves show the Sun glint reflectance calculated by using the MERIS algorithm (second and third reprocessing), and the vertical lines show the edges of the MERIS medium and high glint regions.

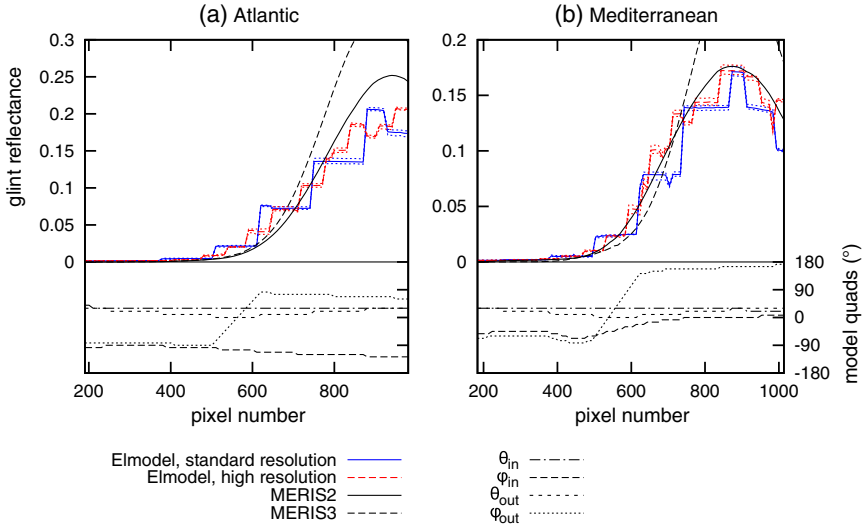

Fig. 8. Glint reflectance at 443 nm estimated by using the elevation-based model with standard and high angular resolution. Results are the mean for five surfaces; the minimum and maximum values are also shown. (a) Values for the Atlantic image and (b) for the Mediterranean. The wind speed was taken as 5 $m\,s^{-1}$ for all pixels.

Running the model at higher angular resolution smoothed some of the variation in the simulated glint reflectance, but did not change the overall size or distribution (Fig. 8). A further preliminary trial was carried out for eight pixels from the Atlantic image at 443 nm, using a quad size of 1° zenith between 25° and 35°, 5° elsewhere, and 2° azimuth. This limited set gave very similar glint reflectance to the values in Fig. 8.

4. Summary and Conclusions

A radiative transfer model that includes sea surface elevation as well as slope has been used to simulate the position and intensity of Sun glint in two MERIS images. The results have been compared to calculations of glint made with the current MERIS glint correction algorithm for Case 1 waters, using a variety of values for the slope statistics.

The radiative transfer model gave lower peak glint and higher levels in the medium glint zone than any of the calculation methods tested. The same differences were observed, to a lesser extent, when the model results were compared to an estimate made using the same radiative transfer model with a slope-statistics method used at the air–water interface. The best agreement between the model and calculation methods was reached when using the surface model of Cox and Munk [4] or Bréon and Henriot [7].

The results presented here suggest that elevation-dependent processes could affect the level of Sun glint, and that an elevation-based model could make estimates of Sun glint reflectance that are different from the slope-statistics methods currently used. This initial study included two sample images, with wind speeds below 8 $m\,s^{-1}$. The findings for the two images were similar in spite of differences in latitude, proximity to land, and reported aerosol quantity, but to investigate how widely the conclusion holds the work should be extended to further images with a greater variety of conditions.

Calculation of glint using the model of Ebuchi and Kizu [6] gives a glint pattern that is different from all other models tested and from the results of radiative transfer modeling, especially in the high glint region. We recommend that its adoption for MERIS data processing should be reviewed.

This work was supported by ARGANS Ltd and Great Western Research (Award No. 363). J. Hedley's contribution was partly funded by the NERC (grant NE/E015654/1). MERIS data were provided by the European Space Agency.

References

1. C. Hu, X. Li, W. G. Pichel, and F. E. Muller-Karger, "Detection of natural oil slicks in the NW Gulf of Mexico using MODIS imagery," Geophys. Res. Lett. **36**, L01604 (2009).
2. M. Wang and S. Bailey, "Correction of Sun glint contamination on the SeaWiFS ocean and atmosphere products," Appl. Opt. **40**, 4790–4798 (2001).
3. L. Bourg, F. Montagner, V. Billat, and S. Belanger, "Sun glint flag algorithm," MERIS ATBD 2.13, version 4.3 (7 July 2011), https://earth.esa.int/instruments/meris/atbd/.
4. C. Cox and W. Munk, "Measurement of the roughness of the sea surface from photographs of the Sun's glitter," J. Opt. Soc. Am. **44**, 838–850 (1954).
5. C. Cox and W. Munk, "Statistics of the sea surface derived from Sun glitter," J. Mar. Res. **13**, 198–227 (1954).
6. N. Ebuchi and S. Kizu, "Probability distribution of surface wave slope derived using Sun glitter images from geostationary meteorological satellite and surface vector winds from scatterometers," J. Oceanogr. **58**, 477–486 (2002).
7. F. Bréon and N. Henriot, "Spaceborne observations of ocean glint reflectance and modeling of wave slope distributions," J. Geophys. Res. Oceans **111**, C06005 (2006).
8. H. Zhang and M. Wang, "Evaluation of Sun glint models using MODIS measurements," J. Quant. Spectrosc. Radiat. Transfer **111**, 492–506 (2010).
9. F. Steinmetz, P. Deschamps, and D. Ramon, "Atmospheric correction in presence of Sun glint: application to MERIS," Opt. Express **19**, 9783–9800 (2011).

10. R. Doerffer, H. Schiller, J. Fischer, R. Preusker, and M. Bouvet, "The impact of Sun glint on the retrieval of water parameters and possibilities for the correction of MERIS scenes," presented at 2nd MERIS/(A)ATSR User Workshop, ESA/ESRIN Frascati, Rome, Italy, 22–26 Sept. 2008.
11. R. Doerffer, "Alternative atmospheric correction procedure for case 2 water remote sensing using MERIS," MERIS ATBD 2.25, version 1.0 (2011), https://earth.esa.int/instruments/meris/atbd/.
12. D. Müller and H. Krasemann, *Product validation and algorithm selection report (PVASR) part 1 atmospheric correction* (ESA, 2012), www.esa-oceancolour-cci.org.
13. C. D. Mobley and L. K. Sundman, *Hydrolight 5 users' guide* (Sequoia, 2008), http://www.sequoiasci.com/products/hl-radiative.cmsx.
14. S. Kay, J. Hedley, S. Lavender, and A. Nimmo-Smith, "Light transfer at the ocean surface modeled using high resolution sea surface realizations," Opt. Express **19**, 6493–6504 (2011).
15. F. Montagner, V. Billat, and S. Belanger, "Sun glint flag algorithm," MERIS ATBD 2.13 (2003), https://earth.esa.int/instruments/meris/atbd/atbd_2_13.pdf.
16. C. Mobley, *Light and Water: Radiative Transfer in Natural Waters* (Academic, 1994).
17. J. Hedley, "PlanarRad User Manual," http://www.planarrad.com.
18. J. Hedley, "PlanarRad software," (2011), http://fsf.nerc.ac.uk/resources/software/planarrad/planarrad.shtml.
19. T. Elfouhaily, B. Chapron, K. Katsaros, and D. Vandemark, "A unified directional spectrum for long and short wind-driven waves," J. Geophys. Res. Oceans **102**, 15781–15796 (1997).
20. M. Heron, W. Skirving, and K. Michael, "Short-wave ocean wave slope models for use in remote sensing data analysis," IEEE Trans. Geosci. Remote Sens. **44**, 1962–1973 (2006).
21. B. Mayer and A. Kylling, "Technical note: the libRadtran software package for radiative transfer calculations—description and examples of use," Atmos. Chem. Phys. **5**, 1855–1877 (2005).
22. B. Mayer, A. Kylling, C. Emde, U. Hamann, and R. Buras, "libRadtran user's guide for libRadtran version 1.7," (2012), www.libradtran.org/doc/libRadtran.pdf.
23. R. H. Grant, G. M. Heisler, and W. Gao, "Photosynthetically-active radiation: sky radiance distributions under clear and overcast conditions," Agric. For. Meteorol. **82**, 267–292 (1996).
24. H. Gordon and K. Voss, *MODIS normalized water-leaving radiance algorithm theoretical basis document*, ATBD-MOD 18 (NASA, 2004), http://modis.gsfc.nasa.gov/data/atbd/ocean_atbd.php.
25. P. Koepke, "Effective reflectance of oceanic whitecaps," Appl. Opt. **23**, 1816–1824 (1984).
26. ACRI, "MERIS level 1 detailed processing model" (2006) http://earth.esa.int/pub/ESA_DOC/ENVISAT/MERIS/Meris_DPM_L1b_i8r0.pdf.